Journal of New Materials for Electrochemical Systems 16, 209-215 (2013)

Electrodeposition of ZnO for Application in Dye-sensitized Solar Cells

F.I. Lizama Tzec[1], M.A. Aguilar Frutis[2], G. Rodríguez Gattorno[1] and G. Oskam[1,*]

[1]Department of Applied Physics, CINVESTAV-IPN, Mérida, Yuc. 97310, México.
[2]CICATA-IPN, Unidad Legaria, México D.F., 11500, México.

Received: October 15, 2012, Accepted: January 21, 2013, Available online: July 04, 2013

Abstract: *ZnO has been electrodeposited from 0.5 M $Zn(NO_3)_2$ at pH 4.5 with and without polyethylene glycol (PEG) as additive. Cyclic voltammetry on FTO substrates reveals two electrochemical regimes, where reduction of nitrate and water are rate determining, respectively. ZnO films were galvanostatically electrodeposited as a function of the deposition current density: at low current densities, where nitrate reduction is rate determining, highly crystalline ZnO films were obtained, whereas amorphous ZnO films were obtained at higher current densities, where water reduction dominates. The amorphous films transform to crystalline ZnO upon sintering, and SEM images show that the presence of PEG results in a homogeneous film morphology. The films were used for the fabrication of dye-sensitized solar cells (DSSCs), resulting in solar cell conversion efficiencies of up to 1.4% for non-sintered ZnO films deposited at low current density (without PEG), while the best cells were obtained with films electrodeposited from the plating bath with 0.15 mM PEG with efficiencies of up to 1.8% for sintered films prepared at higher current density. These results illustrate that the presence of PEG in the plating bath optimizes the film morphology and, hence, the performance of ZnO-based dye-sensitized solar cells.*

Keywords: Cothodic electrodeposition; nanostructured ZnO; Dye-sensitized solar cells; morphology determing additive; PEG.

1. INTRODUCTION

Solar cells based on dye-sensitized, nanostructured metal oxides are promising devices for low-cost solar energy conversion [1]. Figure 1 shows the general structure of the dye-sensitized solar cell (DSSC) device, illustrating the most important processes. The cells are fabricated in a sandwich-type structure between two glass supports coated on one side with a transparent conducting oxide (TCO), generally the lower-cost fluor-doped tin oxide (FTO). The conducting side of one of the glass substrates is coated with a mesoporous layer of metal oxide nanoparticles with a band gap larger than about 3 eV (TiO_2 or ZnO) [2], which is subsequently immersed in a solution containing a dye. The dye molecules are generally anchored to the metal oxide surface through ester-type bonding by condensation of carboxylic acid moieties on the dye with hydroxyl groups on the oxide. The conducting side of the other glass substrate is covered with a thin layer of platinum nanoparticles, which catalyzes the charge transfer from FTO to the electron acceptor in the solution, usually I_3^- [3]. Light is absorbed by the adsorbed dye molecules, and an electron is injected from the excited state into the conduction band of the metal oxide nanomaterial. The dye is regenerated by electron transfer from a reducing agent in solution, generally I^-, which is oxidized to I_3^-. The photoelectrochemical cell is fully regenerative as no chemical changes occur during cell operation. [4].

The metal oxide nanomaterial is employed as a high surface area substrate material to allow for a large number of adsorbed dye molecules, and also plays the role of electron conductor in order to collect the injected electrons in the external circuit. The most commonly used material is TiO_2, which is chemically stable, non toxic and inexpensive. TiO_2 has a band gap of 3.0 - 3.2 eV and a bulk electron mobility of 0.1 - 4 $cm^2 V^{-1} s^{-1}$. An attractive alternative material is ZnO, which has a band gap of 3.2 - 3.3 eV and electron mobility of 200-300 $cm^2 V^{-1} s^{-1}$ in bulk materials and up to 1000 $cm^2 V^{-1} s^{-1}$ in nanowires; these superior electron transport properties make ZnO attractive as an alternate material for DSSC [5-8]. The best efficiency reported for the TiO_2-based DSSC is 12.3% [9] where the nanostructured film is deposited using a screen-printing method, while the record for ZnO is about 6.6% [10]. ZnO is a material with a larger reactivity than TiO_2, which has as advantage that it can be easily synthesized in a variety of nanometric shapes,

*To whom correspondence should be addressed: Email: oskam@mda.cinvestav.mx
Phone: +52 999 9429429; Fax: +52 999 9812917

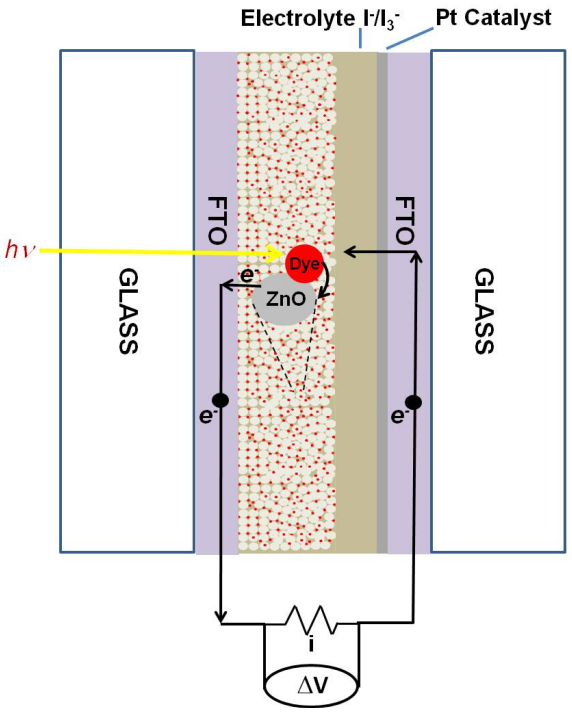

Figure 1. Schematic illustration of a DSSC: light is absorbed by a molecular dye adsorbed to a nanocrystalline, mesoporous ZnO electrode, followed by the injection of an electron into the ZnO conduction band. The dye is regenerated by the electron donor in the electrolyte solution, generating an electron acceptor. The electron is transported through the external circuit and is transferred to the electron acceptor in the solution at the counter electrode, thus closing the loop.

however, ZnO is often unstable in acidic dye solutions, such as the commonly used N3 or N719 dyes [11, 12].

One of the advantages of ZnO is that mesoporous, nanostructured films can be prepared by electrodeposition at ambient pressure and temperature; in addition, the process is much faster than the sol-gel route to prepare a screen printing paste via a nanoparticle colloid. Moreover, electrodeposition can directly result in nanocrystalline films thus avoiding high temperature sintering steps, which also implies that this method is suitable for the fabrication of flexible solar cells using TCO-covered plastic substrates. The method can be scaled-up and can be implemented using a wide variety of Zn salts, including $ZnCl_2$ [13-16], $Zn(C_2H_3O_2)_2$ [17-19], and $Zn(NO_3)_2$ [20-28]. The morphology of the nanostructured films can be modulated by controlling the deposition parameters, and a wide variety of morphologies such as nanotubes, nanobelts, nanowires and nanoparticles have been reported [29].

Electrodeposition of ZnO films occurs through the electrochemical reduction of precursors generating hydroxyl ions, resulting in the deposition of $Zn(OH)_2$ on the electrode surface. The $Zn(OH)_2$ material is subsequently dehydrated to ZnO [30] through a condensation reaction that proceeds through oxolation [31]. There are several options for the source of both the zinc ions and the hydroxyl ions: equations 1 and 2 show a route where $Zn(NO_3)_2$ is used. In this case, the reduction of nitrate to nitrite generates two hydroxyl anions at the electrode surface, and Zn^{2+} ions combine with hydroxyl anions as $Zn(OH)_2$ through an acid-base reaction [32] resulting in precipitation of the material on the electrode surface:

$$NO_3^- + H_2O + 2e^- \rightarrow NO_2^- + 2OH^- \quad (1)$$

$$Zn^{2+} + 2OH^- \rightarrow Zn(OH)_2 \rightarrow ZnO + H_2O \quad (2)$$

The complete reaction can be represented as follows:

$$Zn^{2+} + NO_3^- + 2e^- \rightarrow ZnO + NO_2^- \quad (3)$$

The reaction mechanism and kinetics depend on the pH and precursor concentrations. Nitrate reduction can result in a variety of products and, in order to obtain mainly NO_2^- and OH^-, the nitrate concentration should be high and the pH of the bath should be in the range of 4 - 5 [33,34]. Another electrochemical reaction leading to the indirect synthesis of ZnO is the reduction of water, which generates hydrogen gas and hydroxyl anions; the hydroxyl anions can again combine with Zn^{2+} ions at the electrode surface, eventually generating ZnO [35]. For ZnO electrodeposition in this regime, additives are often used to reduce the absorption of hydrogen in the film [36, 37] and to assist the detachment of bubbles; in addition, the presence of the additive may further refine the pore size [38], which is beneficial for application in the solar cell.

In this work, we report on the electrodeposition of ZnO films from zinc nitrate solution under two different regimens: (i) at relatively low current density where nitrate reduction is the rate-limiting step, and (ii) at high current density where the reduction of water dominates. The morphology of the mesoporous, nanostructured films and the performance of dye-sensitized ZnO solar cells based on the two types of film are compared and related.

2. EXPERIMENTAL

Bath characterization was achieved by cyclic voltammetry, and the electrodeposition experiments were performed in a three-electrode cell configuration, using an FTO-covered glass substrate as working electrode with 0.5 cm^2 of area exposed to the solution. The counter electrode was a large area platinum foil and Ag/AgCl (3 M NaCl) was used as the reference electrode as shown in Figure 2. The baths were prepared with ACS reagent grade chemicals and experiments were performed at room temperature. ZnO films were electrodeposited galvanostatically from 0.5 M $Zn(NO_3)_2$ at pH 4.5, without or with addition of PEG 3,400, using an Autolab 302N electrochemical set-up; the reference electrode is used to monitor the working electrode potential in the three-electrode set-up. All experiments were performed at room temperature and without agitation. After deposition the layer thickness was measured by profilometry (Dektak 3, Veeco), and the films were sensitized with N719 dye (Solaronix) for 3 hours by immersion in 0.5 mM dye solution in ethanol. The time of immersion in the dye solution was optimized by preparing cells with films exposed to the dye solution for different times, and determining the optimal solar cell performance. The amount of dye adsorbed was determined using UV-Vis spectrophotometry (Agilent 8453, diode array spectrophotometer) by desorbing sensitized films in a 0.01 M NaOH solution of a small, fixed volume. The electrodeposited films were studied by

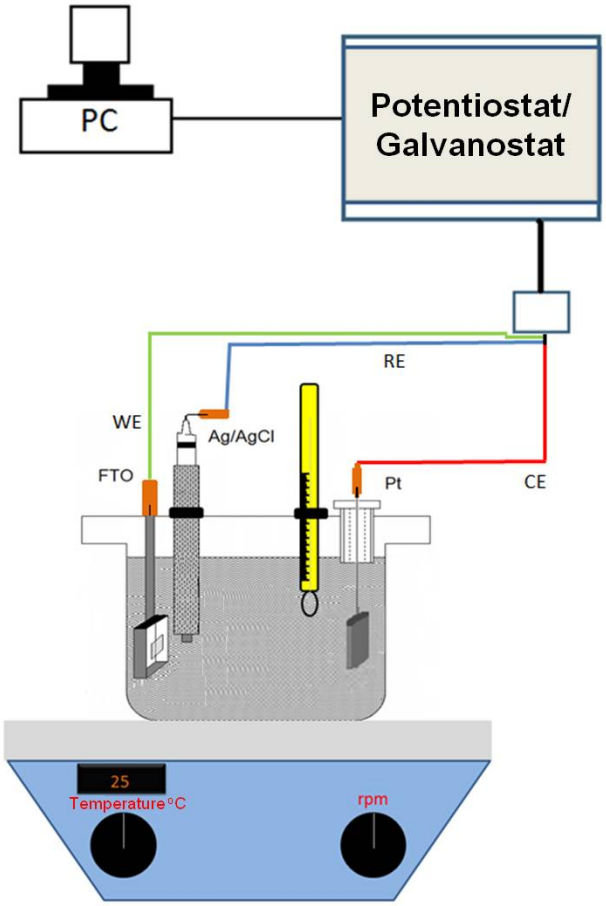

Figure 2. Schematic illustration of the experimental setup employed both for recording the (i,V) curves in the potentiostatic mode, and for the electrodeposition of ZnO films in the galvanostatic mode; in the latter case, the reference electrode was used to monitor the working electrode potential during deposition.

scanning electron microscopy (SEM) (Philips XL-30), X-ray diffraction (Siemens D-5000) and the thermal properties were measured with TGA/DTA (TA Instruments, TG-Q5000).

Solar cells were assembled in a sandwich structure of the FTO/ZnO/dye films and platinum-catalyzed FTO, using Surlyn sealant (DuPont; 60 µm). After sealing, the cell was filled with electrolyte solution through small holes previously perforated in the counter electrode. The electrolyte solution consisted of 0.6 M DMPII, 0.1 M LiI, 0.1 M GuSCN, 0.05 M I_2, and 0.5 M tert-butyl pyridine in 85:15 v/v acetonitrile - valeronitrile. The cell efficiency was determined using a calibrated Xenon lamp (Oriel) in combination with an AM 1.5G filter at 1 sun (100 mW/cm^2); the system was calibrated by adjusting the light intensity using the AM 1.5G filter in combination with a Schott KG5 filter to 28 mW/cm^2, which corresponds to the intensity of the solar spectrum in the wavelength range defined by the two filters. Note that the KG5 filter is removed upon measuring the response of the solar cell. The photocurrent-voltage curve was measured with an Autolab 302N at 5 mV/s using the general set-up as shown in Figure 3.

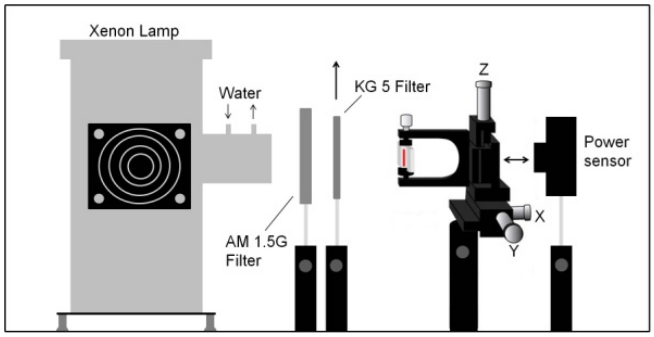

Figure 3. Schematic illustration of the experimental set-up for the characterization of the solar cells, using a Xenon arc lamp, and optical filters to control the lamp spectrum and light intensity. The intensity was calibrated by using the AM1.5G filter in combination with a KG5 filter, while for the solar cell measurements only the AM1.5G filter was employed.

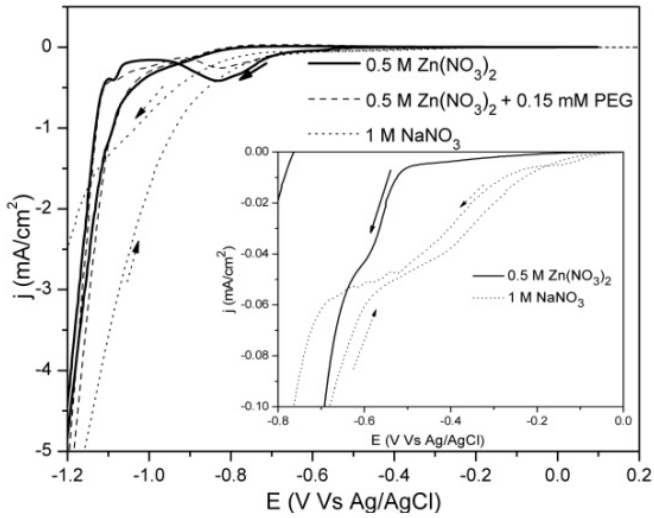

Figure 4. Cyclic voltammetry for FTO electrodes in 0.5 M $Zn(NO_3)_2$ at pH 4.5 with and without 0.15 mM PEG at room temperature and without agitation; the scan rate was 0.8 mV/s.

3. RESULTS AND DISCUSSION

Figure 4 shows cyclic voltammetry curves for 0.5 M $Zn(NO_3)_2$ at pH 4.5 with and without 0.15 mM PEG using FTO as the working electrode. For comparison, an (i,V) curve is also shown for a 1 M $NaNO_3$ solution at the same pH, and taking into account that the redox potential is -0.19 V(Ag/AgCl), it can be concluded that the reduction kinetics of nitrate are very slow. Reduction of water is observed starting at -1.2 V(Ag/AgCl), illustrating that both reactions are not favorable on the FTO surface. In the $Zn(NO_3)_2$ solution, however, the current onset at about -0.5 V(Ag/AgCl) is related to the reduction of nitrate catalyzed by the presence of Zn^{2+} in the solution, and the subsequent deposition of $Zn(OH)_2$ and ZnO as expressed by eq. (2). A current peak is observed, which can be explained by the formation of a somewhat passivating film on the

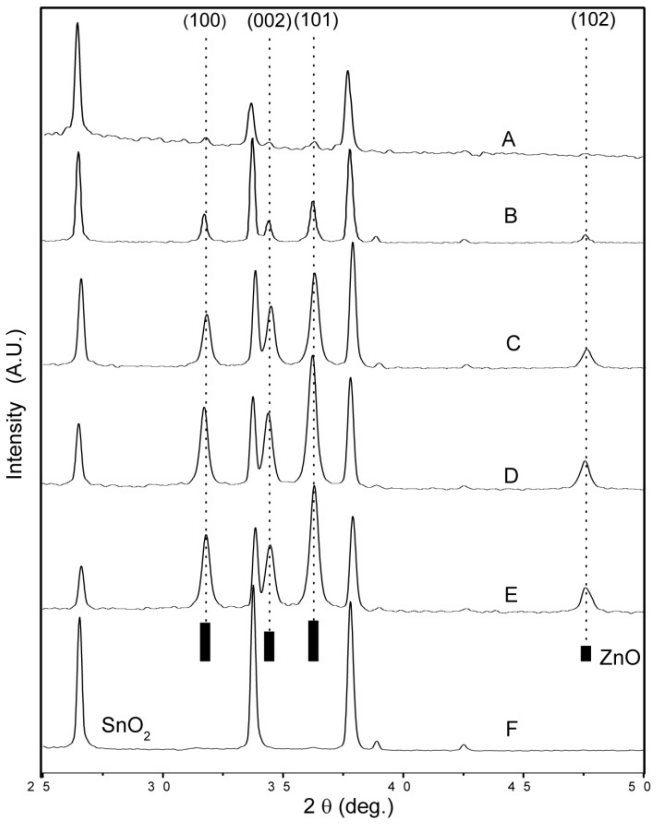

Figure 5. X-ray diffraction patterns of ZnO films galvanostatically electrodeposited on FTO from 0.5 M $Zn(NO_3)_2$ at pH 4.5 at room temperature and without agitation, under the following conditions: (A) at -1 μA/cm^2 from a plating bath with 0.15 mM PEG, and not sintered; (B) at -1 μA/cm^2 from a plating bath with 0.15 mM PEG and sintered for 1 hour at 450 ^oC; (C) at -10 μA/cm^2; (D) at -30 μA/cm^2; (E) at -50 μA/cm^2; the films in (C), (D), and (E) were deposited from a plating bath without PEG and were not sintered. Curve (F) shows the FTO diffraction pattern corresponding to the electrode substrate.

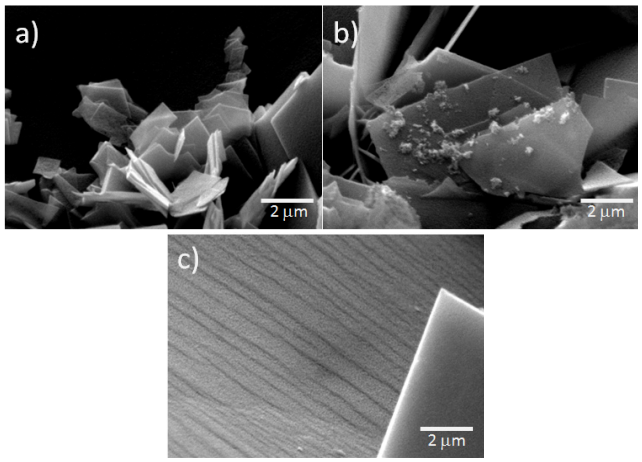

Figure 6. SEM images of ZnO films electrodeposited on FTO from 0.5 M $Zn(NO_3)_2$ at pH 4.5 as a function of the current density, in the regime where nitrate reduction is rate determining, and the films are crystalline as-deposited: (a) -50 μA/cm^2; (b) -30 μA/cm^2; (c) -10 μA/cm^2.

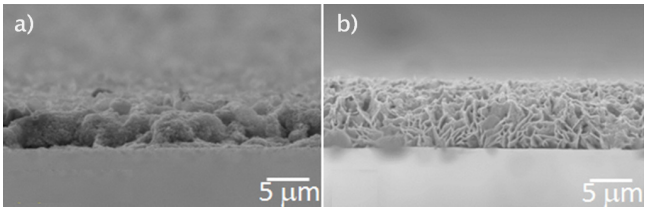

Figure 7. SEM images of ZnO films electrodeposited on FTO at room temperature and without agitation at -1 mA/cm^2 from a 0.5 M $Zn(NO_3)_2$ bath at pH 4.5: (a) without PEG and, (b) with 0.15 mM PEG. The charge passed through the system was Q = -2.6 C/cm^2. The films were sintered for 1 hour at 450 ^oC.

FTO surface. The second scan shows a shift of the current onset to more negative potential, indicating a similar inhibiting effect. At more negative potentials, bubbles were observed at the electrode surface and water reduction is the dominant process. At around -1.15 V(Ag/AgCl) the surface turned dark, which is most likely related to the deposition of amorphous $Zn(OH)_2$. It should be noted that it has been reported that the reduction of Zn^{2+} to metallic Zn (E_0 = -0.96 V(Ag/AgCl)) is generally not observed in baths with a high nitrate concentration [39]. The addition of PEG to the deposition bath results in a slight decrease in the current density in the potential range where nitrate reduction dominates, but not to a major shift of the onset potential.

The X-ray diffraction patterns obtained for films prepared by electrodeposition at different current densities are shown in Figure 5. In all cases, the amount of charge passed through the circuit was -1.3 C/cm^2, which would correspond to a film thickness of 1 μm if one assumes that reaction (3) takes place with 100% efficiency, that the film is compact and consists of ZnO. At larger current density, where water reduction is the dominating process, deposition from a bath with $Zn(NO_3)_2$ and PEG results in mainly amorphous films (A) with traces of ZnO that transform to ZnO upon sintering at 450 ^oC for 60 min (B). At very low current densities, where only nitrate reduction takes place, polycrystalline ZnO was obtained without any need for sintering. The average crystallite size obtained from the peak width and using the Scherrer equation was 21 nm for layer B, 11 nm for the layer C and 9 nm for layers D and E.

Figure 6 shows SEM images of electrodeposited ZnO films obtained from a $Zn(NO_3)_2$ bath without PEG at low current densities, where the reduction of nitrate is rate limiting, as a function of the current density. The electrodeposits consist of a hexagonal sheet type of morphology, while the characteristic size of the features decreases with increasing current density. SEM images of the morphology of sintered ZnO films on FTO that were electrodeposited in the higher current density regime, where the reduction of water dominates, for deposition solutions without and with the additive PEG are shown in Figure 7. The images illustrate the effect of the presence of PEG: the film morphology obtained from the bath

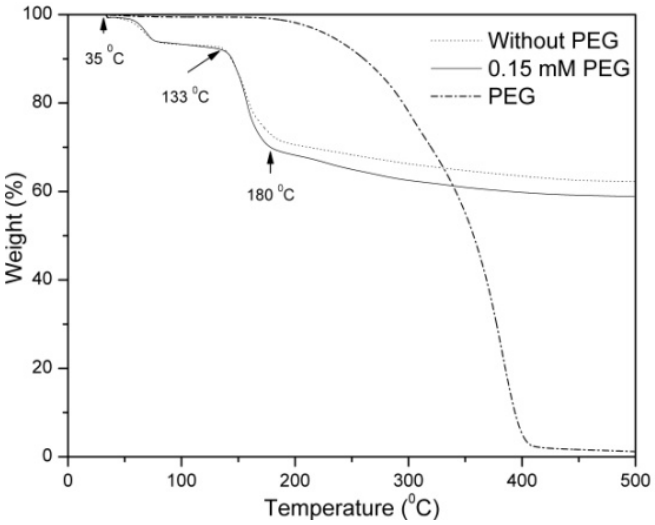

Figure 8. Thermogravimetric analysis for electrodeposited ZnO films from 0.5 M $Zn(NO_3)_2$ at pH 4.5 with and without 0.15 mM PEG. The deposition current density was -1 mA/cm^2. The heating rate was 10 °C/min and the measurements were performed in a N_2 atmosphere. The curve for only PEG is also shown for comparison.

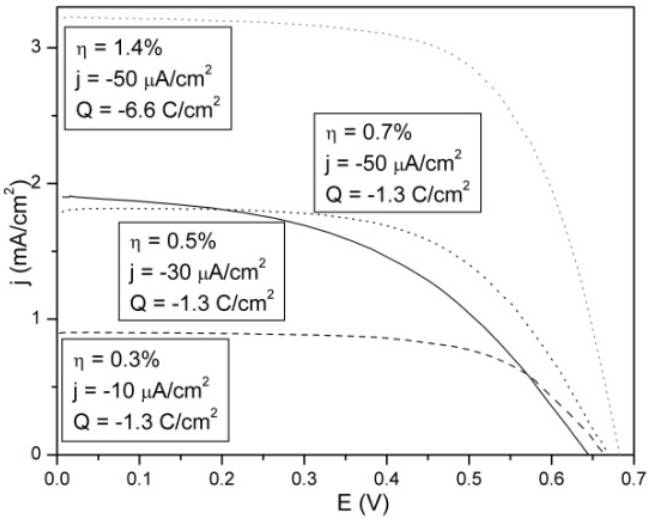

Figure 9. (i,V) curves obtained for DSSCs constructed with ZnO films on FTO electrodeposited from 0.5 M $Zn(NO_3)_2$ at pH 4.5 in function of the current density and deposition charge as indicated.

without PEG can be described as rather compact with an irregular surface, and consisting of aggregated leaves. The film obtained from the bath with PEG shows a more open morphology, with a regular surface structure and consisting of well-defined ZnO flakes. The deposition charge was -2.6 C/cm^2, which corresponds to a film thickness of 2 μm assuming a 100% current efficiency for the deposition process and a compact ZnO film. It can be seen that the film thickness is 5 - 10 μm, which indicates that reaction (3) does not adequately describe the deposition process and/or a significant

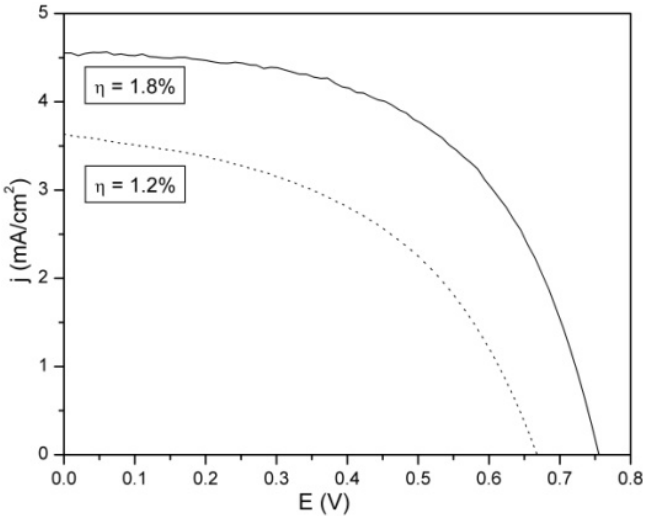

Figure 10. Current - voltage curves obtained for DSSCs constructed with ZnO films electrodeposited at larger current density from 0.5 M $Zn(NO_3)_2$ without (dashed line) and with 0.15 mM PEG (solid line), after sintering. The current density was -1 mA/cm^2 and the electrodeposition charge was -2.6 C/cm^2; the average thickness determined with profilometry was 10 μm.

porosity of the films. Note that for application in the dye-sensitized solar cell, it is essential to be able to electrodeposit porous films, as opposed to for most applications of electrodeposition. The ZnO films corresponding to the images in Figure 7 were analyzed with UV-Vis absorbance spectroscopy, by immersing the films in a dye solution to color the films and subsequent desorption to obtain information on the surface area of the films. It was found that the absorbance was about 10% higher for the film prepared by electrodeposition from the bath with PEG, indicating that the films have a slightly larger surface area.

Thermogravimetric analysis (TGA) of the electrodeposited ZnO films obtained from plating baths with and without PEG is shown in Figure 8. For both types of film, weight loss is observed between 50 °C and 130 °C related to the removal of absorbed water, while a pronounced weight loss between 130 °C and 180 °C is related to removal of adsorbed crystal water molecules [40-43]. Beyond 180 °C a weight change is observed that is significantly more pronounced in the sample obtained from the bath with PEG. The results suggest that this can be attributed to the removal of organic matter; the TGA results for PEG powder shows that the polymer decomposes in the temperature range of 180 - 400 °C. It can be concluded that PEG is incorporated in the ZnO film, indicating that PEG is a morphology determining agent even at the very low concentration of 0.15 mM PEG in the plating bath.

Figure 9 shows the (i,V) curves obtained for DSSCs fabricated with ZnO films electrodeposited from a 0.5 M $Zn(NO_3)_2$ bath without PEG at low current densities, where nitrate reduction is rate limiting, and with a morphology as shown in Figure 6. For the three different current densities, the same charge density of -1.3 C/cm^2 was employed. The figure shows that the conversion efficiency of the solar cells depends on the electrodeposition current density,

with the best results obtained for 50 μA/cm^2 with an efficiency of 0.7%. For the deposition at 50 μA/cm^2, cells were also prepared with films corresponding to a deposition charge of -6.6 C/cm^2, and it can be seen that the efficiency is twice as large at 1.4%, indicating that further optimization of these cells is possible. It should be emphasized that these films were not sintered and can, hence, be used on plastic, flexible FTO-coated plastic films. The electrodeposition time is a somewhat complicating factor, though, as deposition took between 7 and 36 hours, due to the very low deposition current densities used.

The (i,V) curves obtained for solar cells prepared with ZnO films that were electrodeposited in the regime where the water reduction reaction dominates are shown in Figure 10. In this case, the films were sintered for 1 hour at 450 ^{o}C in order to obtain crystalline ZnO, and the morphology corresponds to the images in Figure 7. It can be seen that the short circuit current and efficiency improve compared to the cells prepared with films deposited in the nitrate reduction regime. The improvement can be related with the morphology of these films, which show a more porous and open structure. The film thickness determined with profilometry was about 10 μm for the deposition charge of -2.6 C/cm^2, hence, it can be concluded that the films are significantly porous. The presence of PEG can affect the film morphology in a variety of ways, related to adsorption on the surface and incorporation into the film. Upon application of the current, ZnO nucleation occurs on sites that are not blocked by PEG. During the growth of the nuclei, PEG may be adsorbed on preferential sites allowing growth mainly in two directions, thus forming well-defined flakes. Furthermore, PEG acts as a surfactant thus promoting the early detachment of the gas bubbles formed during the process, which could lead to better mechanical stability of the films. Finally, the TGA measurements show that despite the low concentration of PEG in the plating bath, a significant amount of PEG is incorporated into the porous film, which can subsequently be removed by sintering. As a consequence, the morphology of the films is better defined and more homogeneous as compared to the films deposited from plating baths without PEG.

4. CONCLUSIONS

Voltammetry on FTO electrodes in 0.5 M $Zn(NO_3)_2$ baths at pH 4.5 with or without 0.15 mM PEG shows that there are two main electrochemical processes. The reduction of nitrate was observed starting at an onset potential of about -0.5 V(Ag/AgCl), exhibiting slow reaction kinetics. The second process is the reduction of water at more negative potentials. Electrodeposition in the kinetically-limited nitrate reduction regime from the solution without PEG produces highly crystalline ZnO films consisting of flakes with a feature size decreasing with increasing deposition current density. Solar cells fabricated with these electrodeposited ZnO films, without any sintering step, showed efficiencies of up to 1.4%, depending on the deposition current density and the charge passed through the system. Films electrodeposited at higher current densities, in the regime where water reduction dominates, were amorphous, and transformed into crystalline ZnO films after sintering for 1 hour at 450 ^{o}C. The homogeneity of the film morphology was found to improve significantly when a low concentration of PEG was added to the plating bath, resulting in a film consisting of well-defined flakes. TGA/DTA analysis showed that PEG is incorporated in the film, and using UV-Vis spectrophotometry it was found that the surface area of the sintered film was slightly larger for the films deposited from the plating bath with PEG. Solar cells prepared with the ZnO films electrodeposited from the plating bath with PEG showed the best characteristics with an efficiency of up to 1.8% for an approximately 10 μm thick film.

5. ACKNOWLEDGEMENTS

We gratefully acknowledge financial support from the Consejo Nacional de Ciencia y Tecnología (CONACYT, Mexico) under grant 80002-Y and 178510, from FORDECYT project 116157 (LENERSE), and from FOMIX-Yucatán under grant 170120.

REFERENCES

[1] B. O'Regan and M. Grätzel, Nature, 353, 737 (1991).
[2] G. Oskam, Curr. Top. Electrochem., 10, 141 (2004).
[3] A. Hagfeldt, G. Boschloo, L.K.L. Sun and H. Pettersson, Chem. Rev., 110, 6595 (2010).
[4] E. Guillén, F. Casanueva, J.A. Anta, A. Vega-Poot, G. Oskam, R. Alcántara, C. Fernández-Lorenzo and J. Martín-Calleja, J. Photochem. Photobiol. A: Chem., 200, 364 (2008).
[5] C. Bauer, G. Boschloo, E. Mukhtar and A. Hagfeldt, J. Phys. Chem. B, 105 (2001).
[6] D.C. Look, D.C. Reynolds, J.R. Sizelove, R.L. Jones, C.W. Litton, G. Cantwell and W.C. Harsch, Solid State Commun., 105, 399 (1998).
[7] R. Katoh, A. Furube, A.V. Barzykin, H. Arakawa and M. Tachiya, Coord. Chem. Rev., 248, 1195 (2004).
[8] C.H. Seager and S.M. Myers, J. Appl. Phys., 94 (2003).
[9] A. Yella, H.-W. Lee, H.N. Tsao, C. Yi, A.K. Chandiran, M.K. Nazeeruddin, E.W.-G. Diau, C.-Y. Yeh, S.M. Zakeeruddin and M. Gratzel, Science, 334, 629 (2011).
[10] M. Saito and S. Fujihara, Energy Environ. Sci., 1, 280 (2008).
[11] K. Keis, C. Bauer, G. Boschloo, A. Hagfeldt, K. Westermark, H. Rensmo and H. Siegbahn, J. Photochem. Photobiol. A: Chem., 148, 57 (2002).
[12] R. Katoh, A. Furube, T. Yoshihara, K. Hara, G. Fujihashi, S. Takano, S. Murata, H. Arakawa and M. Tachiya, J. Phys. Chem. B, 108, 4818 (2004).
[13] R. Tena-Zaera, J. Elias, G. Wang and C. Levy-Clement, J. Phys. Chem. C, 111, 16706 (2007).
[14] B. Canava and D. Lincot, J. Appl. Electrochem., 30, 711 (2000).
[15] Y. Feng, W. Xindong, Y. Zhuanyu, L. Jingjing, L. Caishun and W. Tongtao, Rare Metals, 27, 513 (2008).
[16] E. Rayon, J. Cembrero and B. Mari, Mater. Lett., 64, 2601 (2010).
[17] A.I. Inamdar, S.H. Mujawar, S.B. Sadale, A.C. Sonavane, M.B. Shelar, P.S. Shinde and P.S. Patil, Sol. Energy Mater. Sol. Cells, 91, 864 (2007).
[18] A.I. Inamdar, S.H. Mujawar, S.R. Barman, P.N. Bhosale and P.S. Patil, Semicond. Sci. Technol., 23, 085013 (2008).
[19] S. Yamabi and H. Imai, J. Mater. Chem., 12, 3773 (2002).
[20] F. Wang, R. Liu, A. Pan, L. Cao, K. Cheng, B. Xue, G. Wang, Q. Meng, Q.L.J. Li, Y. Wang and B.Z.T. Wang, Mater. Lett.,

61, 2000 (2007).
[21]J. Lee, S.C. Nam and Y. Tak., Korean J. Chem. Eng., 22, 161 (2005).
[22]J. Zhao, J. Zheng-Guo, T. Li, L. Xiao-Xin and L. Zhi-Feng, J. Am. Ceram. Soc., 89, 2654 (2006).
[23]M. Izaki and T. Omi, J. Electrochem. Soc., 143, L53 (1996).
[24]M. Izaki and Y. Saijo, J. Electrochem. Soc., 150, C73 (2003).
[25]O.W.J.S. Rutten, A.V. Sandwijk and G.V. Weert, J. Appl. Electrochem., 29, 87 (1999).
[26]K.-S. Choi and E.M.P. Steinmiller, Electrochim. Acta, 53, 6953 (2008).
[27]F.I. Lizama-Tzec and G. Oskam, ECS Transactions, 25, 45 (2010).
[28]K. Nomura, N. Shibata and M. Maeda, J. Electrochem. Soc., 7, F76 (2002).
[29]L. Lijuan, L. Gang, L. Bihui, C. Zhenghua and T. Yiwen, Wuhan Univ. J. Nat. Sci., 115, 130 (2010).
[30]S. Otani, J. Katayama, H. Umemoto and M. Matsuoka, J. Electrochem. Soc., 153, C551 (2006).
[31]J.-P. Jolivet, M. Henry and J. Livage, Metal oxide chemistry and synthesis from solution to solid state, John Wiley & Sons (2000).
[32]K. Murase, H. Tada, T. Shinagawa, M. Izaki and Y. Awakura, J. Electrochem. Soc., 153, C735 (2006).
[33]M.T. de Groot and M.T.M. Koper, J. Electroanal. Chem., 562, 81 (2004).
[34]C. Milhano, D. Pletcher and R.E. White, The electrochemistry and electrochemical technology of nitrate, p. 1, Springer New York, 2009.
[35]Y.Y. Xi, Y.F. Hsu, A.B. Djurisic and W.K. Chan, J. Electrochem. Soc., 155, D595 (2008).
[36]J.C. Ballesteros, P. Díaz-Arista, Y. Meas, R. Ortega and G. Trejo, Electrochim. Acta, 52, 3686 (2007).
[37]J. Chen, S.K. Spear, J.G. Huddleston and R.D. Rogers, Green Chem., 7, 64 (2005).
[38]F.I. Lizama-Tzec and G. Oskam, ECS Transactions, 41, 47 (2012).
[39]T. Yoshida, D. Komatsu, N. Shimokawa and H. Minoura, Thin Solid Films, 451, 166 (2004).
[40]A.T. Cursino, A.S. Mangrich, J.E. Gardolinski, N. Mattoso and F. Wypych, J. Braz. Chem. Soc., 22, 1183 (2011).
[41]A. Velasco, T. Oguchi and K. Hee-Joon, J. Cryst. Growth, 311, 2731 (2009).
[42]E.J. Griffith, Anal. Chem., 29, 198 (1957).
[43]N. Kanari, D. Mishra, I. Gaballah and B. Dupré, Thermochim. Acta, 410, 93 (2004).